

CHALMERS
UNIVERSITY OF TECHNOLOGY

Transmit and Receive Beamforming for In-Band Full-Duplex MU-MIMO under Self-Interference Constraints with Measurement-Based Validation

Downloaded from: https://research.chalmers.se, 2026-11-22 21:15 UTC

Citation for the original published paper (version of record):
Ayebe, M., Maaskant, R., Goransson, B. et al (2026). Transmit and Receive Beamforming for In-Band Full-Duplex MU-MIMO under Self-Interference Constraints with Measurement-Based Validation. IEEE Open Journal of Antennas and Propagation, 7(5): 1702-1711. http://dx.doi.org/10.1109/OJAP.2026.3715376

N.B. When citing this work, cite the original published paper.

© 2026 IEEE. Personal use of this material is permitted. Permission from IEEE must be obtained for all other uses, in any current or future media, including reprinting/republishing this material for advertising or promotional purposes, or reuse of any copyrighted component of this work in other works.

(article starts on next page)

Received 2 June 2026; revised 13 July 2026; accepted 16 July 2026. Date of publication 20 July 2026; date of current version 23 October 2026.

Digital Object Identifier 10.1109/OJAP.2026.3715376

Transmit and Receive Beamforming for In-Band Full-Duplex MU-MIMO Under Self-Interference Constraints With Measurement-Based Validation

MUSTAFA AYEBE[1] (Student Member, IEEE), ROB MAASKANT[1] (Senior Member, IEEE), BO GÖRANSSON[2] (Member, IEEE), AND HENRIK HOLTER[2] (Member, IEEE)

[1]Antenna Systems Group, Department of Electrical Engineering, Chalmers University of Technology, SE-412 96 Göteborg, Sweden
[2]Radio and Antennas Research Group, AI and Technology Foresight, Ericsson AB, SE-164 83 Stockholm, Sweden

CORRESPONDING AUTHOR: MUSTAFA AYEBE (e-mail: mustafa.ayebee@gmail.com)

This work was supported by the Advanced Digitalization Program at the Wireless Infrastructure Technology at Chalmers (WiTECH) Centre (Digital Antenna ARRAYs (DIGIARRAY) Project) funded by Vinnova, Ericsson, and Chalmers.

ABSTRACT In-band full-duplex (IBFD) multi-user multiple-input multiple-output (MU-MIMO) systems are fundamentally limited by self-interference (SI) caused by strong transmitter-to-receiver coupling, which can degrade receiver performance and restrict simultaneous uplink and downlink operation. This work presents a measured-coupling-based transmit and receive beamforming framework for IBFD MU-MIMO arrays with separate transmit and receive apertures. The transmit design restricts excitation to a low-coupling spatial subspace derived from measured coupling characteristics, ensuring controlled SI levels while maintaining sufficient spatial degrees of freedom for multi-user downlink beamforming. Channel state information is assumed available at the transmitter and represented in the angular domain, enabling beamforming based on dominant spatial directions without requiring uplink–downlink reciprocity. At the receiver, residual SI is mitigated through subspace projection before uplink combining. Full-wave simulations and experimental validation on an RFSoC-based testbed with strongly coupled Vivaldi transmit/receive arrays at 3 GHz demonstrate that imposing a 45 dB isolation threshold at the transmit beamforming stage increases per-element isolation from approximately 20–40 dB to 60–80 dB while maintaining multi-beam operation. Subsequent receive beamforming further suppresses residual SI, yielding over 80 dB of system-level isolation. Frequency-dependent evaluation shows that the center-frequency beamformers maintain effective isolation over the operating bandwidth. These results confirm a scalable and hardware-efficient approach for SI mitigation in IBFD MU-MIMO systems under strong mutual coupling conditions.

INDEX TERMS In-band full-duplex, multi-user MIMO, self-interference mitigation, beamforming, antenna array, RFSoC.

I. INTRODUCTION

IN-BAND full-duplex (IBFD) communication enables simultaneous transmission and reception over the same frequency band, potentially doubling spectral efficiency compared to conventional half-duplex systems [1], [2]. Beyond improved spectrum utilization, IBFD supports low-latency bidirectional links, higher base station (BS) capacity through concurrent uplink and downlink transmission, and joint communication and sensing functionalities. When combined with multiple-input multiple-output (MIMO) techniques, IBFD systems exploit spatial multiplexing and beamforming to improve throughput and interference management. These advantages are further enhanced in MIMO architectures, where large antenna arrays provide high beamforming gain, efficient interference suppression via linear processing, and reduced per-antenna transmit power [3].

Despite these advantages, realizing them in practical multi-antenna IBFD systems remains fundamentally constrained by self-interference (SI), where strong transmit (Tx) signals leak into the receive (Rx) chain and can overwhelm desired signals, as well as by hardware nonidealities. In large antenna arrays, SI is further aggravated by mutual coupling, near-field propagation effects, element-pattern variations, and radiative and conductive leakage, which degrade Tx-to-Rx isolation,

© 2026 The Authors. This work is licensed under a Creative Commons Attribution 4.0 License.
For more information, see https://creativecommons.org/licenses/by/4.0/

array gain, and receiver dynamic range [4]. These challenges arise regardless of whether the system operates in single-user or multi-user MIMO (MU-MIMO) modes. In IBFD MU-MIMO deployments, however, the simultaneous transmission and reception of multiple spatial streams over the same frequency band further complicates beamforming design. SI suppression must therefore be achieved while preserving spatial multiplexing gains and controlling inter-user crosstalk. As the number of antennas grows relative to the number of served users, per-element analog SI cancellation becomes increasingly impractical due to hardware complexity, calibration overhead, cost, and power consumption [5], [6].

Prior works have addressed SI mitigation across propagation, analog, and digital domains [7]. Propagation-based techniques—such as physical separation [8], cross-polarization [9], circulator [10], and defective ground plane [11]—provide initial isolation but deteriorate in reflective environments and large antenna arrays. Analog cancellers subtract reconstructed SI replicas and can achieve substantial suppression [12]; however, their hardware complexity and calibration requirements scale poorly with antenna count. Digital beamforming methods, such as SoftNull, mitigate SI through precoding and baseband processing but may sacrifice array or multiplexing gain due to optimization trade-offs [13]. Hybrid analog-digital architectures reduce RF-chain requirements, yet often rely on iterative optimization that can converge to suboptimal solutions, particularly in sub-connected arrays prone to self-nulling [14]. More recent constrained minimum mean-square error precoding [15] and nulling steering beamforming [16] have shown improved SI rejection, but they either operate in single-user scenarios or require per-angle search mechanisms. Learning-based approaches improve robustness to nonlinearities and time-varying SI, while reciprocity-based schemes enhance spectral efficiency; however, many assume idealized SI suppression [17], [18]. In [19], a joint Tx–Rx beamforming approach demonstrates more than 80 dB SI suppression under experimental conditions; nevertheless, the method is limited to single-beam, single-user IBFD systems. Scalable and hardware-efficient SI mitigation, therefore, remains an open challenge in IBFD MU-MIMO systems.

To address these challenges, this work presents a measurement-driven beamforming framework for IBFD MU-MIMO systems that jointly integrates SI control, multi-user beamforming, and spatial multiplexing through an explicit spatial-subspace formulation. The proposed framework first constructs a low-coupling Tx subspace directly from the measured Tx–to–Rx coupling characteristics, enforcing a user-selectable receiver-protection isolation constraint while preserving the remaining spatial degrees of freedom (DoF) for simultaneous multi-user transmission. Zero-forcing (ZF) precoding is then performed within this feasible Tx subspace to suppress inter-user downlink interference. At the receiver, residual SI is further mitigated by projecting the received signal onto the orthogonal complement of the dominant interference subspace before conventional uplink combining. Both Tx and Rx beamforming weights are obtained in closed form directly from the measured coupling and communication channel matrices, avoiding iterative optimization and enabling computationally efficient implementation. The framework is validated through full-wave simulations and experimental measurements using a radio frequency system-on-chip (RFSoC)-based testbed with strongly coupled Vivaldi Tx/Rx arrays, demonstrating stable multi-user beamforming operation and SI suppression under realistic conditions.

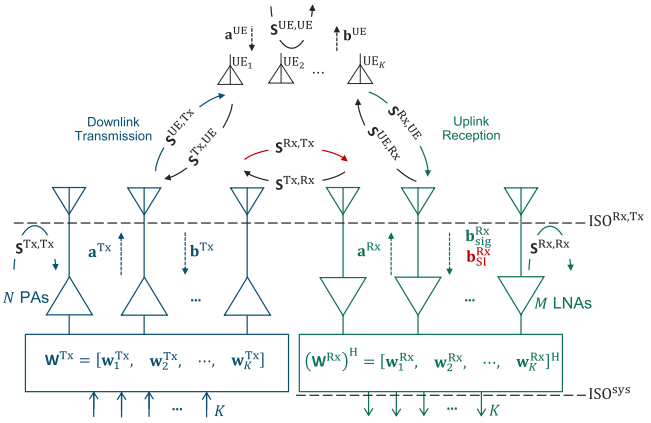


FIGURE 1. IBFD MU-MIMO communication setup featuring an *N*-element Tx and an *M*-element Rx array. During downlink transmission, the Tx array generates *K* independent beams directed toward the UEs. Simultaneously, in uplink reception, the Rx array synthesizes *K* beams to capture uplink signals from the UEs. Owing to the IBFD operation, the Rx array also experiences SI originating from the Tx array.

The remainder of the paper is organized as follows. Section II presents the IBFD MU-MIMO system model and definitions. Section III formulates the ZF-based Tx and Rx beamforming design, including SI control mechanisms. Section IV provides proof-of-concept simulation results, followed by experimental validation and case-study analysis in Section V. Conclusions are drawn in Section VI.

Notations: A, a, $\hat{\mathbf{a}}$, and a denote a matrix, a vector, a unit vector, and a scalar, respectively. The conjugate, transpose, and Hermitian transpose are represented by $(\cdot)^*$, $(\cdot)^{\mathrm{T}}$, and $(\cdot)^{\mathrm{H}}$. The operators $|\cdot|$ and $\|\cdot\|_2$ denote scalar magnitude and Euclidean norm. The identity matrix of size $N \times N$ is denoted by I_N.

II. SYSTEM MODEL AND DEFINITIONS

We consider a MU-MIMO IBFD transceiver system, illustrated in Figure 1, where a BS simultaneously serves K single antenna user equipments (UEs). The BS is equipped with an N-element Tx antenna array and an M-element Rx array, each with its own RF front-end chain. The Tx array generates K spatial beams for downlink transmission, while the Rx array forms K beams for uplink reception.

A. OPERATING PRINCIPLE AND COUPLING MECHANISMS

The IBFD MU-MIMO transceiver is modeled using the power-wave and scattering-parameter formalism, where the a- and b-waves represent the incident and reflected power

waves at the front-end ports [20]. The analysis is conducted under the SI dominant regime, where thermal noise and external noise contributions are neglected for tractability.

The BS transmits the complex baseband symbol vector $\mathbf{s} \in \mathbb{C}^{K\times 1}$ intended for the downlink users. The incident power-wave vector at the Tx array ports is expressed as

$$\mathbf{a}^{\mathrm{Tx}} = S_{21}^{\mathrm{PA}}\,\mathsf{W}^{\mathrm{Tx}}\mathbf{s} \quad \in \mathbb{C}^{N\times 1}, \tag{1}$$

where $\mathsf{W}^{\mathrm{Tx}} \in \mathbb{C}^{N\times K}$ is the Tx beamforming (precoding) matrix with unit-norm column vectors satisfying $\|\mathbf{w}_k^{\mathrm{Tx}}\|_2 = 1$, $\forall k$. The parameter S_{21}^{PA} represents the forward transmission coefficient of the power amplifiers (PAs), which are assumed identical, linear, and narrowband across all Tx chains. The total available power at the Tx ports is then

$$P_{\mathrm{av}} = \frac{1}{2}\left(\mathbf{a}^{\mathrm{Tx}}\right)^{\mathrm{H}}\mathbf{a}^{\mathrm{Tx}}. \tag{2}$$

To simplify the analysis, we assume negligible reflections at the low-noise amplifier (LNA) inputs at the BS, i.e., $\mathbf{a}^{\mathrm{Rx}} = \mathbf{0}$. This assumption is consistent with well-matched receiver front-end designs, where LNAs feature high input return loss, effectively eliminating reflections back toward the antenna/RF chain. Furthermore, we assume that the UE terminals support IBFD operation with well-matched RF front-ends. In line with practical full-duplex designs employing impedance matching networks and circulators to suppress internal reflections, the self-scattering matrix at the UE can be approximated as $\mathsf{S}^{\mathrm{UE,UE}} = \mathbf{0}$. Under these assumptions, the outgoing power waves at the downlink users originate solely from the BS Tx array and are given by

$$\mathbf{b}^{\mathrm{UE}} = \mathsf{S}^{\mathrm{UE,Tx}}\,\mathbf{a}^{\mathrm{Tx}}, \tag{3}$$

where $\mathsf{S}^{\mathrm{UE,Tx}} \in \mathbb{C}^{K\times N}$ is the Tx-to-UE coupling matrix. The SI wave component (red in Figure 1) at the Rx array ports due to simultaneous downlink transmission is expressed as

$$\mathbf{b}_{\mathrm{SI}}^{\mathrm{Rx}} = \mathsf{S}^{\mathrm{Rx,Tx}}\mathbf{a}^{\mathrm{Tx}}. \tag{4}$$

where $\mathsf{S}^{\mathrm{Rx,Tx}} \in \mathbb{C}^{M\times N}$ is the Tx-to-Rx coupling matrix in the IBFD configuration, accounting for radiative and conductive coupling, near-field interactions, and hardware leakage. The total coupled power at the Rx array is then

$$P_{\mathrm{coup}} = \frac{1}{2}\left(\mathbf{b}_{\mathrm{SI}}^{\mathrm{Rx}}\right)^{\mathrm{H}}\mathbf{b}_{\mathrm{SI}}^{\mathrm{Rx}} = \frac{1}{2}\left(\mathbf{a}^{\mathrm{Tx}}\right)^{\mathrm{H}}\left(\boldsymbol{S}^{\mathrm{Rx,Tx}}\right)^{\mathrm{H}}\boldsymbol{S}^{\mathrm{Rx,Tx}}\mathbf{a}^{\mathrm{Tx}}. \tag{5}$$

Importantly, P_{coup} depends only on the Tx beamformer and is independent of the Rx beamforming matrix. Therefore, the design of W^{Tx} governs SI mitigation at the Rx ports and helps prevent front-end saturation. Even when saturation effects are avoided, residual SI power can still exceed the desired uplink signal by several orders of magnitude. Therefore, Rx beamforming is essential for further SI suppression and for preserving receiver sensitivity. Accordingly, the total post-LNA SI power and the desired uplink signal power for user k after Rx beamforming are defined as

$$P_{\mathrm{SI}} = \frac{1}{2}\left|S_{21}^{\mathrm{LNA}}\right|^2\left\|\left(\mathsf{W}^{\mathrm{Rx}}\right)^{\mathrm{H}}\mathbf{b}_{\mathrm{SI}}^{\mathrm{Rx}}\right\|_2^2, \tag{6}$$

$$P_{\mathrm{sig},k} = \frac{1}{2}\left|S_{21}^{\mathrm{LNA}}\right|^2\left|\left(\mathbf{w}_k^{\mathrm{Rx}}\right)^{\mathrm{H}}\mathbf{b}_{\mathrm{sig}}^{\mathrm{Rx}}\right|^2, \tag{7}$$

where $\mathsf{W}^{\mathrm{Rx}} \in \mathbb{C}^{M\times K}$ is the Rx beamforming matrix with unit-norm columns, and S_{21}^{LNA} is the forward transmission coefficient of the LNAs, assumed identical, linear, and narrowband. The received uplink signal wave vector (green in Figure 1) at the Rx ports is

$$\mathbf{b}_{\mathrm{sig}}^{\mathrm{Rx}} = \mathsf{S}^{\mathrm{Rx,UE}}\mathbf{a}^{\mathrm{UE}} \in \mathbb{C}^{M\times 1}, \tag{8}$$

depicting the superposition of signals from uplink users. Here, $\mathsf{S}^{\mathrm{Rx,UE}} \in \mathbb{C}^{M\times K}$ is the UE-to-Rx coupling matrix.

B. DEFINITION OF COUPLING MATRICES BETWEEN BS AND UES

This subsection characterizes the electromagnetic coupling between the BS antenna arrays and the UEs. The coupling matrices are constructed using embedded element patterns (EEPs), which naturally incorporate mutual coupling effects within multi-port antenna structures. The formulation is general and applies to both BS arrays and UE terminals.

1) Tx Embedded Element Patterns: Let $E_n^{\mathrm{Tx}}(\mathbf{r})$ denote the co-polarized component[1] of the radiated far-field generated by the n-th Tx element and evaluated at the observation point $\mathbf{r}$ referenced to the local origin $\mathcal{O}_n$ of that element. The scalar quantity $r = \|\mathbf{r}\|_2$ represents the distance from $\mathcal{O}_n$ to the observation point, and λ denotes the wavelength. As shown in Fig. 2(a), the n-th embedded Tx element pattern in the observation direction $\hat{\mathbf{r}}$ is obtained by exciting the n-th element with a unit incident power wave ($a_n^{\mathrm{Tx}} = 1$) while terminating all other elements in their characteristic impedances [21]. The Tx EEP is defined as

$$g_n^{\mathrm{Tx}}(\hat{\mathbf{r}}) = E_n^{\mathrm{Tx}}(\mathbf{r})\,r\,e^{j2\pi r/\lambda}. \tag{9}$$

Here, the factor r compensates for the $1/r$ far-field amplitude decay, while the exponential term removes the free-space propagation phase shift, yielding the intrinsic complex angular response of the embedded Tx element.

2) Rx Embedded Element Patterns: Let $g_m^{\mathrm{Rx}}(\hat{\mathbf{r}})$ denote the co-polar component of the m-th Rx EEP in the observation direction $\hat{\mathbf{r}}$, defined when all array ports are terminated in their characteristic impedances, as shown in Figure 2(b). Consider an incident plane wave whose complex envelope is evaluated at the local origin $\mathbf{r}_m \equiv \mathcal{O}_m$ of the m-th Rx element, denoted by $E^{\mathrm{i}}(\mathbf{r}_m)$. The resulting outgoing wave at the m-th Rx port is then given by

$$b_m^{\mathrm{Rx}} = g_m^{\mathrm{Rx}}(\hat{\mathbf{r}}) \cdot E^{\mathrm{i}}(\mathbf{r}_m). \tag{10}$$

Note that $g_m^{\mathrm{Rx}}(\hat{\mathbf{r}})$ is defined directly as a *receiving pattern* under normalized incident field from different directions such that $|E^{\mathrm{i}}| = 1$ V/m, rather than being obtained from the transmitting EEP via reciprocity.

3) BS–UE Electromagnetic Coupling Under line-of-sight propagation: We first consider the downlink transmission (see Figure 2(c)) and neglect higher-order mutual coupling

[1]Co-polar component: the component of the radiated or received electromagnetic field aligned with the intended antenna polarization.

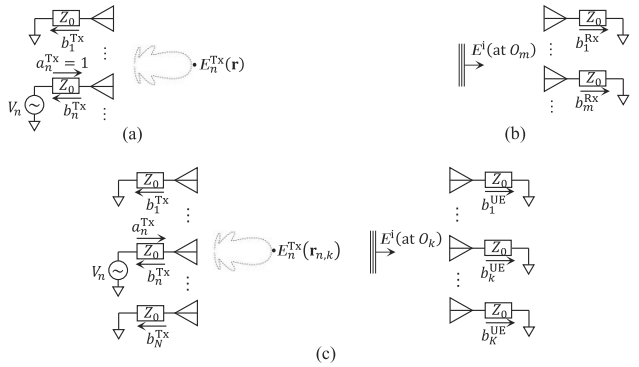


FIGURE 2. (a) Tx EEP definition; (b) Rx EEP definition; (c) BS Tx–UE propagation scenario.

terms between the BS and the UEs. Let $\mathbf{r}_n$ and $\mathbf{r}_k$ denote the position vector of the local origin $\mathcal{O}_n$ of the n-th BS Tx element and $\mathcal{O}_k$ of UE k, respectively. Based on the Tx EEP definition, the radiated field produced by the n-th BS element and evaluated at the UE local origin $\mathcal{O}_k$ is

$$E_n^{\mathrm{Tx}}(\mathbf{r}_{n,k}) = g_n^{\mathrm{Tx}}(\hat{\mathbf{r}}_{n,k})\, r_{n,k}^{-1}\, e^{-j2\pi r_{n,k}/\lambda}\, a_n^{\mathrm{Tx}}, \tag{11}$$

where $r_{n,k} = \|\mathbf{r}_n - \mathbf{r}_k\|_2$ and a_n is the incident power wave exciting the n-th BS Tx element. This radiated field is the incident field seen by user k, such that (s.t.), $E^{\mathrm{i}}(\mathbf{r}_k) = E_n^{\mathrm{Tx}}(\mathbf{r}_{n,k})$. Substituting this incident field into the Rx EEP relation in Eq. (10) yields the outgoing wave at UE k,

$$b_k^{\mathrm{UE}} = g_k^{\mathrm{URx}}(-\hat{\mathbf{r}}_{n,k})\, g_n^{\mathrm{Tx}}(\hat{\mathbf{r}}_{n,k})\, r_{n,k}^{-1}\, e^{-j2\pi r_{n,k}/\lambda}\, a_n^{\mathrm{Tx}}, \tag{12}$$

where the minus sign in the argument of $g_k^{\mathrm{URx}}(\cdot)$ reflects evaluation of the UE receiver pattern in the wave arrival direction, which is opposite to the BS-to-user propagation direction $\hat{\mathbf{r}}_{n,k}$. Consequently, the (k,n)-th entry of the Tx-to-UE coupling matrix is

$$S_{k,n}^{\mathrm{UE,Tx}} = g_k^{\mathrm{URx}}(-\hat{\mathbf{r}}_{n,k})\, g_n^{\mathrm{Tx}}(\hat{\mathbf{r}}_{n,k})\, r_{n,k}^{-1}\, e^{-j2\pi r_{n,k}/\lambda}. \tag{13}$$

We next consider uplink reception, following an analogous procedure to the downlink case. Let $r_{m,k} = \|\mathbf{r}_m - \mathbf{r}_k\|_2$ denote the distance between the k-th user and the m-th BS Rx element. The (m,k)-th element of UE-to-Rx coupling matrix, $\mathbf{S}^{\mathrm{Rx,UE}}$ is therefore

$$S_{m,k}^{\mathrm{Rx,UE}} = g_m^{\mathrm{Rx}}(-\hat{\mathbf{r}}_{m,k})\, g_k^{\mathrm{UEtx}}(\hat{\mathbf{r}}_{m,k})\, r_{m,k}^{-1}\, e^{-j2\pi r_{m,k}/\lambda}, \tag{14}$$

where $g_k^{\mathrm{UEtx}}(\cdot)$ is the UE transmitter pattern.

C. RADIATED POWER AND REALIZED GAIN

For a downlink UE located in the direction $\hat{\mathbf{r}}_k$, the *embedded-element steering vector* of the Tx array is defined as

$$\mathbf{g}_k^{\mathrm{Tx}} = \left[g_1^{\mathrm{Tx}}(\hat{\mathbf{r}}_{1,k}), \cdots, g_N^{\mathrm{Tx}}(\hat{\mathbf{r}}_{N,k})\right] \in \mathbb{C}^{1\times N}, \tag{15}$$

The *transmitted effective isotropic radiated power (EIRP) per user* is then

$$\mathrm{EIRP}_k(\hat{\mathbf{r}}_k) = \frac{2\pi}{\eta_0}\left|S_{21}^{\mathrm{PA}}\right|^2 \left|\mathbf{g}_k^{\mathrm{Tx}}\mathbf{w}_k^{\mathrm{Tx}}\right|^2, \tag{16}$$

where η_0 denotes the free-space impedance. To characterize receiver performance, the *partial realized gain* of the Rx beam corresponding to uplink user k is defined as

$$\mathrm{RxGAIN}_k(\hat{\mathbf{r}}_k) = \frac{4\pi}{\lambda^2}\frac{P_{\mathrm{sig},k}}{S_k}, \tag{17}$$

where $S_k = \frac{1}{2\eta_0}\|E_k^{\mathrm{sig}}\|_2^2$ denotes the power flux density of the incident plane wave from uplink user k, defined using Ludwig's third polarization convention (not necessarily polarisation matched to the antenna) [22]. While impedance mismatches may reduce the realized gain in practice, this metric remains a useful and physically meaningful measure for evaluating and optimizing Rx beamformer performance under reasonably well-matched conditions.

D. ISOLATION DEFINITIONS

Based on the above formulation, we adopt several isolation metrics from [19] for the IBFD MU-MIMO system. First, the BS *Rx array antenna isolation* at the LNA inputs, under Tx beamforming W^{Tx}, is defined as follows:

$$\mathrm{ISO}^{\mathrm{Rx,Tx}}(\mathsf{W}^{\mathrm{Tx}}) = \frac{P_{\mathrm{av}}(\mathsf{W}^{\mathrm{Tx}})}{P_{\mathrm{coup}}(\mathsf{W}^{\mathrm{Tx}})}. \tag{18}$$

When monitoring the m-th Rx element individually, with all Tx elements excited, the coupled power at that element is

$$P_{\mathrm{coup},m} = \frac{1}{2}(\mathbf{a}^{\mathrm{Tx}})^{\mathrm{H}}(\mathsf{S}_m^{\mathrm{Rx,Tx}})^{\mathrm{H}}\mathsf{S}_m^{\mathrm{Rx,Tx}}\mathbf{a}^{\mathrm{Tx}}, \tag{19}$$

where $\mathsf{S}_m^{\mathrm{Rx,Tx}} \in \mathbb{C}^{1\times N}$ is the m-th row of the SI coupling matrix $\mathsf{S}^{\mathrm{Rx,Tx}}$. This metric is referred to as the *BS Rx element isolation*. It is always larger than the Rx array-level isolation, since P_{coup} aggregates the coupled power across all Rx ports. This observation motivates setting isolation requirements slightly above the minimum element isolation to ensure robust performance without overdesign.

Finally, the *total IBFD system isolation* at the output of the Rx beamformer is defined as

$$\mathrm{ISO}^{\mathrm{sys}}(\mathsf{W}^{\mathrm{Tx}}, \mathsf{W}^{\mathrm{Rx}}) = \frac{P_{\mathrm{av}}(\mathsf{W}^{\mathrm{Tx}})}{P_{\mathrm{SI}}(\mathsf{W}^{\mathrm{Tx}}, \mathsf{W}^{\mathrm{Rx}})}. \tag{20}$$

III. BEAMFORMING PROBLEM FORMULATION

A. ZFTX BEAMFORMING WITH SI CONTROL

1) IBFD Tx–to–Rx Isolation Control: To control SI at the receiver and enable a constrained spatial design, we impose a minimum Tx-to-Rx isolation threshold κ, defined as a design threshold reflecting a receiver-protection-oriented link-budget constraint:

$$\mathrm{ISO}^{\mathrm{Rx,Tx}}(\mathsf{W}^{\mathrm{Tx}}) \geq \kappa. \tag{21}$$

As enforced by (21), the achieved Rx array isolation is guaranteed to be no less than κ, while higher isolation may be obtained depending on the available spatial subspace. Since κ determines the feasible Tx beamforming subspace, it directly controls the available spatial DoF. The feasible subspace for $\mathbf{a}^{\mathrm{Tx}}$ satisfying (21) is obtained by solving the (generalized) eigenvalue problem:

$$\mathsf{I}_N\,\mathbf{u}_n^{\mathrm{Tx}} = \zeta_n\,(\mathsf{S}^{\mathrm{Rx,Tx}})^{\mathrm{H}}\mathsf{S}^{\mathrm{Rx,Tx}}\,\mathbf{u}_n^{\mathrm{Tx}}, \quad n = 1,\ldots,N, \tag{22}$$

where ζ_n represents the isolation metric, ordered as $\zeta_1 \geq \ldots \geq \zeta_N$. Let L denote the number of eigenvalues satisfying $\zeta_n \geq \kappa$. The corresponding feasible subspace, common to all Tx beams, is then

$$\{\mathbf{w}_k^{\mathrm{Tx}}\}_{k=1}^{K} \in \mathrm{span}\{\mathbf{u}_1^{\mathrm{Tx}}, \mathbf{u}_2^{\mathrm{Tx}}, \ldots, \mathbf{u}_L^{\mathrm{Tx}}\}. \tag{23}$$

Since any linear combination of $\{\mathbf{u}_n^{\mathrm{Tx}}\}_{n=1}^{L}$ will satisfy the isolation constraint, one can also consider Tx beamforming on a beam-to-beam basis, or a linear combination thereof (multi-beam case as discussed above), i.e., for beam k:

$$\mathbf{w}_k^{\mathrm{Tx}} = \mathsf{U}^{\mathrm{Tx}}\boldsymbol{\alpha}_k, \tag{24}$$

where $\mathsf{U}^{\mathrm{Tx}} = [\mathbf{u}_1^{\mathrm{Tx}}, \mathbf{u}_2^{\mathrm{Tx}}, \ldots, \mathbf{u}_L^{\mathrm{Tx}}] \in \mathbb{C}^{N\times L}$ and $\boldsymbol{\alpha}_k \in \mathbb{C}^{L\times 1}$ represents the reduced-dimension coefficient vector. Within this subspace, the minimum achievable isolation is $\zeta_L \geq \kappa$, which holds for any nonzero $\boldsymbol{\alpha}_k$. For a K-user downlink system employing ZF precoding, a necessary condition for feasibility is that the available Tx subspace provides sufficient spatial DoF, i.e., $L \geq K$. If this condition is not satisfied, exact ZF beamforming becomes infeasible. In such cases, the design must either reduce the number of simultaneously served users. This formulation highlights that the Tx beamforming design is fundamentally a spatial DoF-constrained projection problem, in which the effective Tx dimension is reduced from N to L depending on the SI coupling structure and the selected isolation threshold.

2) ZFTx–BF Optimization: In multi-beam downlink transmission, Tx beam k is designed to concentrate energy toward user k located at direction $\hat{\mathbf{r}}_k$. However, beam k may also radiate energy toward other user directions $\{\hat{\mathbf{r}}_j\}_{j\neq k}$, generating BS–to–downlink-user crosstalk. To eliminate inter-user interference while serving multiple users simultaneously, ZF Tx beamforming is applied [23], [24].

In addition to inter-user interference, a portion of the transmitted power can couple into the Rx array, generating SI that degrades IBFD operation. To mitigate this, the Tx excitations are restricted to the subspace spanned by the orthonormal vectors $\{\mathbf{u}_n^{\mathrm{Tx}}\}_{n=1}^{L}$, chosen to control coupling into the Rx array. The resulting reduced-dimension Tx beamforming matrix is

$$\mathsf{A} = \left[\boldsymbol{\alpha}_1, \boldsymbol{\alpha}_2, \cdots, \boldsymbol{\alpha}_K\right] \in \mathbb{C}^{L\times K}, \tag{25}$$

so that the full Tx beamformer is

$$\mathsf{W}^{\mathrm{Tx}} = \mathsf{U}^{\mathrm{Tx}}\mathsf{A}. \tag{26}$$

The ZF condition requires that all off-diagonal terms of $\mathsf{S}^{\mathrm{UE,Tx}}\mathsf{U}^{\mathrm{Tx}}\mathsf{A}$ vanish, ensuring that each Tx beam directs energy only toward its intended user. This condition is satisfied by solving the unconstrained least-squares problem [25], [26] for the reduced-dimension beamforming matrix $\mathsf{A}_{\mathrm{opt}}$

$$\boldsymbol{A}_{\mathrm{opt}} = \left(\boldsymbol{U}^{\mathrm{Tx}}\right)^{\mathrm{H}}\left(\boldsymbol{S}^{\mathrm{UE,Tx}}\right)^{\mathrm{H}}\left[\boldsymbol{S}^{\mathrm{UE,Tx}}\boldsymbol{U}^{\mathrm{Tx}}\left(\boldsymbol{U}^{\mathrm{Tx}}\right)^{\mathrm{H}}\left(\boldsymbol{S}^{\mathrm{UE,Tx}}\right)^{\mathrm{H}}\right]^{\dagger}. \tag{27}$$

Then, the closed-form Tx array beamformer (precoding) matrix with unit-norm column vectors will be

$$\mathsf{W}_{\mathrm{opt}}^{\mathrm{Tx}} = \mathsf{U}^{\mathrm{Tx}}\mathsf{A}_{\mathrm{opt}} \in \mathbb{C}^{N\times K}, \tag{28}$$

which enforces that the transmitted signal lies entirely in the reduced low-coupled subspace, thereby satisfying the isolation constraint by construction.

B. ZFRX-BEAMFORMING WITH RESIDUAL SI MITIGATION

1) Residual SI Mitigation: At the BS receiver, residual SI must be suppressed to maintain system isolation. For a pre-applied ZFTx beamformer, the system isolation is

$$\mathrm{ISO}^{\mathrm{sys}}\left(\mathsf{W}^{\mathrm{Tx}}, \mathsf{W}^{\mathrm{Rx}}\right) = \frac{\left(\mathbf{a}^{\mathrm{Tx}}\right)^{\mathrm{H}}\mathbf{a}^{\mathrm{Tx}}}{\left|S_{21}^{\mathrm{LNA}}\right|^2 \left\|\left(\mathsf{W}^{\mathrm{Rx}}\right)^{\mathrm{H}}\mathbf{b}_{\mathrm{SI}}^{\mathrm{Rx}}\right\|_2^2}. \tag{29}$$

Maximizing isolation simply requires the Rx beamformers to be orthogonal to $\mathbf{b}_{\mathrm{SI}}^{\mathrm{Rx}}$. Since $\mathbf{b}_{\mathrm{SI}}^{\mathrm{Rx}} \in \mathbb{C}^{M\times 1}$, its orthogonal complement has dimension $M-1$. Let $\mathsf{U}^{\mathrm{Rx}} \in \mathbb{C}^{M\times(M-1)}$ be any orthonormal basis satisfying $\left(\mathbf{b}_{\mathrm{SI}}^{\mathrm{Rx}}\right)^{\mathrm{H}}\mathsf{U}^{\mathrm{Rx}} = \mathbf{0}$. Thus, each Rx beamforming vector can be parameterized as

$$\mathbf{w}_k^{\mathrm{Rx}} = \mathsf{U}^{\mathrm{Rx}}\boldsymbol{\beta}_k \quad \in \mathbb{C}^{M\times 1}, \tag{30}$$

where $\boldsymbol{\beta}_k \in \mathbb{C}^{(M-1)\times 1}$ is the coefficient vector associated with the k-th Rx beam. This parameterization enforces zero projection onto the residual SI direction and eliminates the residual SI component at the receiver, thereby maximizing the achievable system isolation.

2) ZFRx–BF Optimization: For multi-beam uplink reception, ZFRx beamforming is applied to suppress inter-user interference, whereas residual SI is eliminated by restricting $\mathbf{w}_k^{\mathrm{Rx}}$ to U^{Rx}. Collecting the beamforming coefficient vectors for all K uplink users yields

$$\mathsf{B} = \left[\boldsymbol{\beta}_1, \boldsymbol{\beta}_2, \cdots, \boldsymbol{\beta}_K\right] \in \mathbb{C}^{(M-1)\times K}, \tag{31}$$

so that the full Rx beamformer is

$$\mathsf{W}^{\mathrm{Rx}} = \mathsf{U}^{\mathrm{Rx}}\mathsf{B}. \tag{32}$$

Zero inter-user interference is achieved by choosing B such that the off-diagonal terms of $\mathsf{B}^{\mathrm{H}}\left(\mathsf{U}^{\mathrm{Rx}}\right)^{\mathrm{H}}\mathsf{S}^{\mathrm{Rx,UE}}$ vanish. The solution is

$$\boldsymbol{B}_{\mathrm{opt}} = \left(\boldsymbol{U}^{\mathrm{Rx}}\right)^{\mathrm{H}}\boldsymbol{S}^{\mathrm{Rx,UE}}\left[\left(\boldsymbol{S}^{\mathrm{Rx,UE}}\right)^{\mathrm{H}}\boldsymbol{U}^{\mathrm{Rx}}\left(\boldsymbol{U}^{\mathrm{Rx}}\right)^{\mathrm{H}}\boldsymbol{S}^{\mathrm{Rx,UE}}\right]^{\dagger}. \tag{33}$$

The resulting Rx beamforming matrix with unit-norm columns is

$$\mathsf{W}_{\mathrm{opt}}^{\mathrm{Rx}} = \mathsf{U}^{\mathrm{Rx}}\mathsf{B}_{\mathrm{opt}} \in \mathbb{C}^{M\times K}, \tag{34}$$

suppresses residual SI and inter-user interference under perfect channel knowledge assumptions, while preserving the intended array gain toward each uplink user.

IV. PROOF OF CONCEPT: PERFORMANCE EVALUATION

We evaluate the proposed framework via a proof-of-concept simulation using 1×12 ($M = N = 12$) uniform linear arrays at both the Tx and Rx, each composed of Vivaldi antennas (Figure 3). These elements are fed via coaxial probes through the ground plane [27]. The system simultaneously serves $K = 5$ UEs positioned in the far field at specific E-plane angles θ_k and a common distance $r = r_{n,k} = r_{m,k}$. Electromagnetic simulations are performed in CST Studio Suite, with

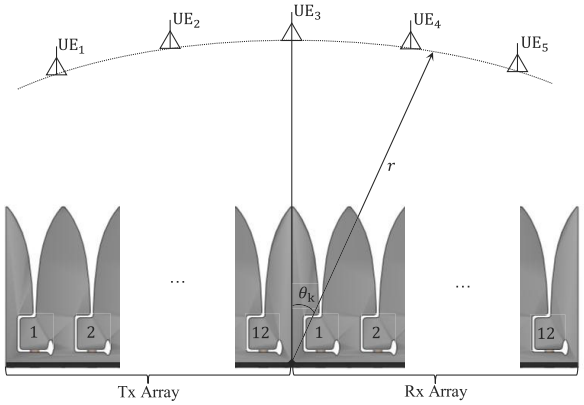


FIGURE 3. IBFD MU-MIMO system with 12-element Tx and 12-element Rx uniform linear arrays using Vivaldi antennas [27]. The Tx array forms 5 E-plane beams toward UEs, while the Rx array forms 5 E-plane beams to receive uplink signals from UEs. All users are assumed to be in the far field at angles θ_k and a common distance r from the arrays.

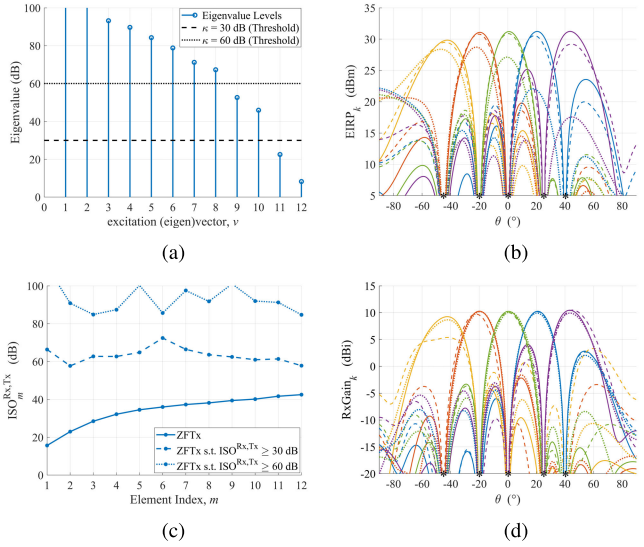


FIGURE 4. (a) Eigenvalue spectrum of $\left[(\mathbf{S}^{\mathrm{Rx,Tx}})^{\mathrm{H}}\mathbf{S}^{\mathrm{Rx,Tx}}\right]^{-1}$; (b) Tx EIRP beampatterns at steering angles $\theta_k = -45^\circ, -20^\circ, 0^\circ, 25^\circ, 40^\circ$ under conventional ZFTx (solid), and ZFTx with isolation constraints $\mathrm{ISO}^{\mathrm{Rx,Tx}} \geq 30$ dB (dashed) and 60 dB (dotted); (c) Corresponding Rx element isolation obtained from the beamforming weights; (d) Rx array beampatterns for the same steering angles under conventional ZFRx (solid) and SI-Null ZFRx applied with ZFTx designs under Tx-side isolation constraints $\mathrm{ISO}^{\mathrm{Rx,Tx}} \geq 30$ dB (dashed) and 60 dB (dotted).

beamforming algorithms implemented in MATLAB. Unless otherwise stated, the performance evaluation is carried out at the center frequency using a single Tx–to–Rx coupling matrix representative of a narrowband condition.

The eigenvalue spectrum of $\left[(\mathbf{S}^{\mathrm{Rx,Tx}})^{\mathrm{H}}\mathbf{S}^{\mathrm{Rx,Tx}}\right]^{-1}$ at 3 GHz, shown in Figure 4(a), characterizes the coupling-dependent spatial DoF used to construct the reduced Tx subspace $\mathbf{U}^{\mathrm{Tx}}$. Larger eigenvalues correspond to weaker coupling modes, while smaller values indicate dominant coupling components. Based on this spectrum, eigenmodes are selectively retained according to thresholds $\kappa = 30$ dB and 60 dB to form reduced-dimensional transmission subspaces. These thresholds serve as representative operating points to illustrate the trade-off between SI suppression and Tx array performance, rather than application-specific design targets.

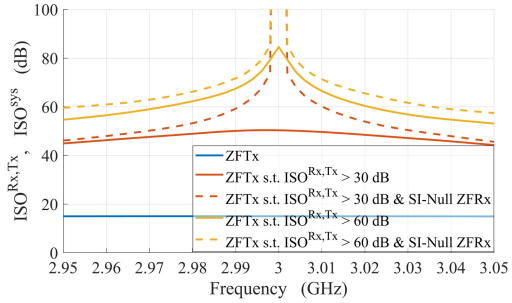


FIGURE 5. Simulated Rx array isolation, $\mathrm{ISO}^{\mathrm{Rx,Tx}}$ (solid lines), and system isolation, $\mathrm{ISO}^{\mathrm{sys}}$ (dashed lines), for $\kappa = 30$ and 60 dB over frequency.

Figure 4(b) compares the Tx EIRP beampatterns of conventional ZFTx and the proposed ZFTx under isolation constraints of 30 dB and 60 dB for five simultaneous downlink users. In both cases, high gain is maintained toward each intended user while preserving the ZF nulls at the locations of the remaining users (marked with asterisks). Enforcing the isolation constraint slightly reduces peak EIRP (by roughly 1–2 dB for the 30 dB case and more noticeably for the 60 dB case) and slightly raises sidelobes, while preserving the main-lobe directions. The performance loss depends on the Tx–to–Rx coupling characteristics (e.g., number of antennas and mutual coupling level) and the number of simultaneously supported beams, reflecting the tradeoff between spatial DoF and enforced isolation constraints.

Figure 4(c) depicts the corresponding Rx element isolation levels. While conventional ZFTx yields approximately 20–40 dB isolation across elements, the constrained designs substantially increase the element isolation, reaching 60–70 dB when enforcing an Rx array isolation constraint of 30 dB and 85–100 dB under the 60 dB constraint, depending on the element index. This improvement directly results from restricting the Tx subspace, which reduces the power projected onto dominant coupling directions.

Figure 4(d) shows the Rx array gain beampatterns for conventional ZFRx and SI-Null ZFRx under constrained ZFTx operation under 30 dB and 60 dB isolation constraints. All beams maintain high gain toward their intended directions while suppressing interference toward other users. Compared to conventional ZFRx, SI-Null ZFRx introduces only minor degradation, except for the $\theta_s = -45^\circ$ case under the 30 dB constraint, where residual coupling from the reduced Tx subspace affects performance. Overall, the results confirm that the receive-side null-space projection effectively mitigates dominant residual SI components.

To characterize the frequency-dependent performance of the center-frequency beamformers, the Tx and Rx coefficients synthesized at $f_c = 3$ GHz are applied across the entire 100-MHz bandwidth. As shown in Figure 5, the center-frequency beamformers remain effective over the operating bandwidth. For the 30 dB Tx isolation constraint, the Rx array isolation varies only slightly across the full 100-MHz

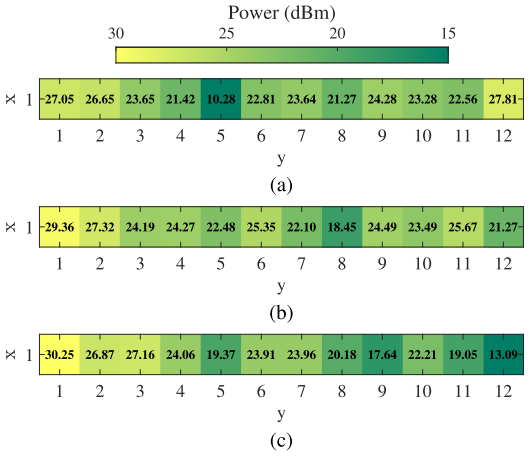


FIGURE 6. Simulated Tx element input power distribution, $\|\mathbf{a}^{\mathrm{Tx}}\|_{\mathrm{dB}}$: (a) conventional ZFTx; (b) ZFTx with $\mathrm{ISO}^{\mathrm{Rx,Tx}} \geq 30$ dB constraint; (c) ZFTx with $\mathrm{ISO}^{\mathrm{Rx,Tx}} \geq 60$ dB constraint.

band. Under the 60 dB constraint, the required Rx array isolation is maintained over approximately 40 MHz, while the overall system isolation is significantly enhanced (>100 dB) within a narrow bandwidth of approximately 2 MHz around f_c. Although the present study focuses on a narrowband proof-of-concept, the proposed framework readily extends to wideband systems by constructing independent reduced Tx and Rx subspaces for each subcarrier (or subband).

The Tx element input power distributions for the three considered ZFTx schemes are compared in Figure 6. In the conventional ZFTx case (a), the power is relatively balanced across the 12 elements, with most values between 21–27 dBm. When a moderate isolation constraint of ≥ 30 dB is imposed (b), the power distribution remains fairly uniform. However, under the stricter isolation requirement of ≥ 60 dB (c), the power becomes significantly more uneven, with several elements, particularly those toward the right side of the array, exhibiting notably lower power levels. This imbalance is an expected consequence of the reduced Tx subspace imposed by the stricter isolation constraint. The resulting power imbalance can be mitigated by relaxing the isolation threshold when additional RF or digital SI cancellation is available, thereby preserving more Tx DoF.

To complement the deterministic performance evaluation, we investigate the impact of hardware-induced perturbations.

A. SENSITIVITY OF ARRAY ISOLATION TO EXCITATION AND COUPLING ERRORS

To assess sensitivity, we consider stochastic perturbations to the Tx excitation vector and the Tx-to-Rx coupling response arising from hardware imperfections and environmental variations. The perturbed quantities are modeled as

$$\mathbf{a}_p^{\mathrm{Tx}} = \mathbf{a}^{\mathrm{Tx}} + \boldsymbol{\delta}_{\mathrm{exc}}, \qquad \mathbf{S}_p^{\mathrm{Rx,Tx}} = \mathbf{S}^{\mathrm{Rx,Tx}} + \boldsymbol{\Delta}_{\mathrm{SI}}, \tag{35}$$

where $\boldsymbol{\delta}_{\mathrm{exc}} \in \mathbb{C}^{N\times 1}$ and $\boldsymbol{\Delta}_{\mathrm{SI}} \in \mathbb{C}^{M\times N}$ represent excitation and coupling perturbations, respectively, with entries modeled as independent complex Gaussian random variables, $\delta_{\mathrm{exc},n} \sim \mathcal{CN}(0, \sigma_{\mathrm{exc}}^2)$ and $\Delta_{\mathrm{SI},mn} \sim \mathcal{CN}(0, \sigma_{\mathrm{SI}}^2)$. The resulting array isolation under perturbations is evaluated using the definition

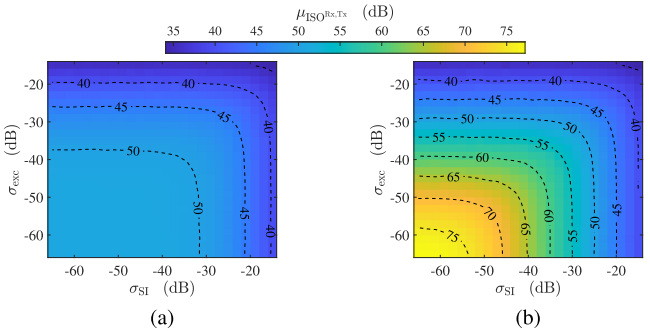


FIGURE 7. Average array isolation, as a function of the standard deviations of Tx excitation and Tx-to-Rx coupling errors. Monte-Carlo results for the ZFTx under: (a) $\mathrm{ISO}^{\mathrm{Rx,Tx}} \geq 30$ dB constraint; (b) $\mathrm{ISO}^{\mathrm{Rx,Tx}} \geq 60$ dB constraint.

in (18). Excitation errors primarily degrade beamforming accuracy, while coupling perturbations directly affect residual SI suppression. This effect becomes more pronounced when $\mathbf{a}^{\mathrm{Tx}}$ is optimized for high isolation, as the reduced nominal coupling power makes the system more sensitive to imperfections.

A Monte-Carlo analysis (1500 trials) shows that both σ_{exc} and σ_{SI} reduce the average array-level isolation $\mu_{\mathrm{ISO}^{\mathrm{Rx,Tx}}}$. As illustrated in Figure 7, the degradation is more pronounced under the stringent $\mathrm{ISO}^{\mathrm{Rx,Tx}} \geq 60$ dB constraint, where the high-isolation region shrinks with increasing error levels. To satisfy this constraint, $\sigma_{\mathrm{exc}} < -39$ dB and $\sigma_{\mathrm{SI}} < -35$ dB are required (see Figure 7(b)). Notably, the element isolation levels remain consistently higher than the corresponding array-level isolation, since the coherent combination of coupling contributions across all Rx elements determines it. These results highlight the tradeoff between nominal isolation performance and sensitivity to hardware non-idealities in IBFD MU-MIMO systems.

V. CASE STUDY AND VALIDATION RESULTS

A. MEASUREMENT SETUP AND CASE STUDY DESCRIPTION

Experimental validation is conducted using the RFSoC-based IBFD platform shown in Figure 8, which extends the system reported in [19] to evaluate the proposed multi-beam ZFTx and ZFRx strategies under controlled two-beam operation in the E-plane. The testbed consists of separate-aperture 3×5 Vivaldi Tx and Rx arrays fabricated using 3D printing and silver coating [27]. The arrays are positioned side-by-side with small inter-array spacing to intentionally create strong near-field coupling and a challenging SI environment.

All measurements are performed inside an anechoic chamber to suppress external reflections and isolate intrinsic Tx-to-Rx coupling. The arrays are connected to a Xilinx Zynq UltraScale+ RFSoC ZCU216 platform, providing multi-channel digital-to-analog conversion (DAC) and analog-to-digital conversion (ADC) interfaces and enabling real-time digital beamforming and baseband processing [28]. The measured responses are calibrated to remove the DAC–ADC frequency response so that only the antenna and propagation characteristics are evaluated. In this setup, no external RF amplification is used; hence $S_{21}^{\mathrm{PA}} = S_{21}^{\mathrm{LNA}} = 1$.

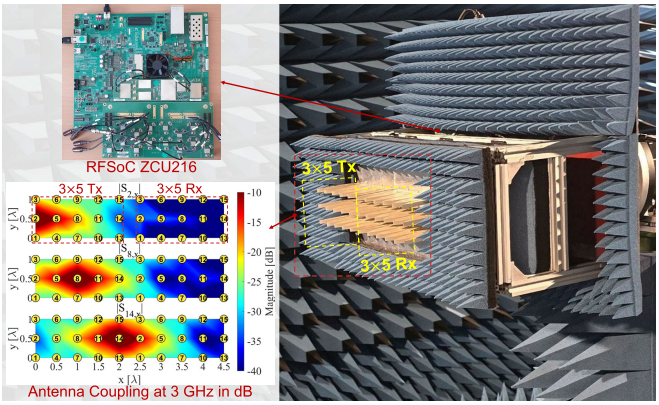


FIGURE 8. Experimental setup used for validating the proposed multi-beam Tx–Rx beamforming framework. The figure is redrawn and summarized based on the measurement platform reported in [19] and illustrates the complete IBFD MU-MIMO system configuration employed in this study.

Prior to the beamforming evaluation, the EEPs of both arrays are characterized using a calibrated movable probe antenna mounted on a positioner. These measurements are used to construct the $\mathbf{S}^{\mathrm{UE,Tx}}$ and $\mathbf{S}^{\mathrm{Rx,UE}}$ matrices.

The Tx-to-Rx coupling matrix is then measured via sequential excitation of each Tx element using the RFSoC DAC chains while recording the corresponding Rx responses through the ADC chains, yielding a full over-the-air multi-port characterization. Since such exhaustive measurements are impractical during real-time operation, the coupling matrix is obtained through an offline calibration procedure and used as the baseline model in this work. In practical deployments, it can instead be estimated using pilot-assisted or reduced-dimensional channel estimation, with estimation errors and hardware non-idealities affecting the accuracy of the constructed low-coupling Tx subspace and the resulting beamforming weights.

Using the measured coupling and EEP matrices, beamforming weights are computed offline and uploaded to the RFSoC platform for real-time validation of the proposed multi-beam ZFTx and ZFRx methods.

B. RESULTS AND DISCUSSION

Figure 9 compares simulated and measured eigenvalue spectra of $\left[(\mathbf{S}^{\mathrm{Rx,Tx}})^{\mathrm{H}}\mathbf{S}^{\mathrm{Rx,Tx}}\right]^{-1}$ at $f_0 = 3$ GHz. The dominant eigenmodes (associated with strong coupling structure) show good agreement between simulation and measurement, while deviations in weaker modes arise from dynamic range limitations, measurement noise, and hardware non-idealities. Based on this spectral behavior, a threshold-based truncation is applied to suppress strong SI modes in the first stage. Specifically, eigenmodes corresponding to isolation levels above a predefined threshold $\kappa = 45$ dB are retained to define the low-coupled Tx subspace.[2]

[2]The threshold κ can generally be defined relative to the Tx power and LNA 1-dB compression point, including modulation backoff. Since no external LNA is used in this setup, $\kappa = 45$ dB is selected empirically to enable controlled comparison between unconstrained and coupling-constrained cases.

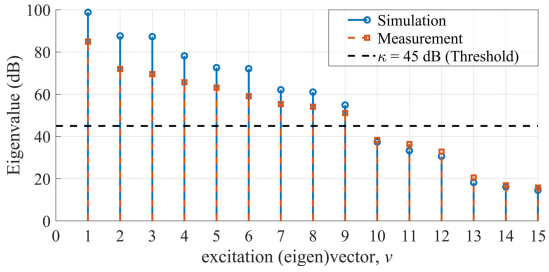


FIGURE 9. Comparison of simulation and measurement: eigenvalue spectrum of $\left[(\mathbf{S}^{\mathrm{Rx,Tx}})^{\mathrm{H}}\mathbf{S}^{\mathrm{Rx,Tx}}\right]^{-1}$.

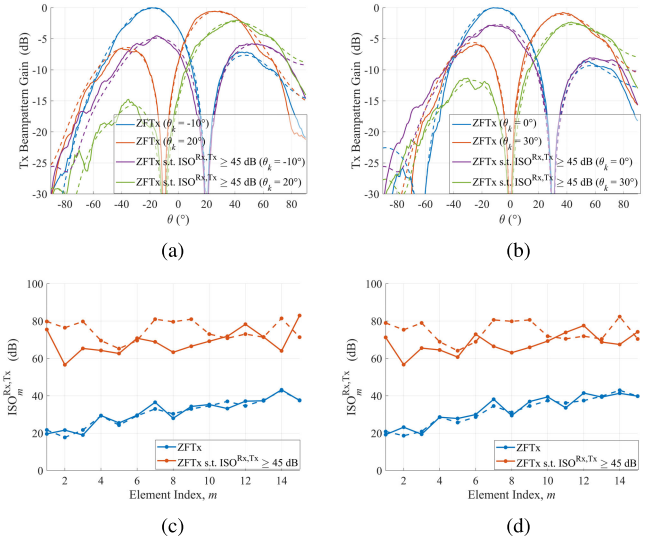


FIGURE 10. Simulation (dashed) and measurement (solid) results for conventional and proposed ZFTx beamformers: normalized Tx gain beam patterns steered to (a) $\theta_k = -10°$ and $\theta_k = 20°$, and (b) $\theta_k = 0°$ and $\theta_k = 30°$; corresponding Rx element isolation resulted from the sum of the associated beamforming weights for (c) $\theta_k = -10°, 20°$, and (d) $\theta_k = 0°, 30°$.

Figures 10(a)–(b) show normalized Tx beampatterns for conventional ZFTx and the proposed constrained ZFTx under $\mathrm{ISO}^{\mathrm{Rx,Tx}} \geq 45$ dB for two representative beam pairs. The constrained solution preserves main-lobe directions and ZF nulls while introducing a 2–5 dB peak gain reduction and slightly elevated sidelobes. Simulation (dashed) and measurement (solid) results show consistent trends, confirming that the constraint reshapes the beam without degrading directional selectivity.

The corresponding Rx element isolation results are shown in Figures 10(c)–(d), where element indexing follows Figure 8. The constraint is applied at the *Rx array level*, i.e., to the total received SI power across all Rx elements rather than per-element isolation. Enforcing $\mathrm{ISO}^{\mathrm{Rx,Tx}} \geq 45$ dB yields significantly improved per-element isolation, typically in the range of 60–80 dB depending on steering direction, corresponding to improvements of up to 50 dB compared to the unconstrained case.

Figures 11(a)–(b) present the measured and simulated Rx beampatterns for conventional ZFRx and SI-Null ZFRx. These results are obtained under the isolation-constrained ZFTx configuration ($\mathrm{ISO}^{\mathrm{Rx,Tx}} \geq 45$ dB), where two

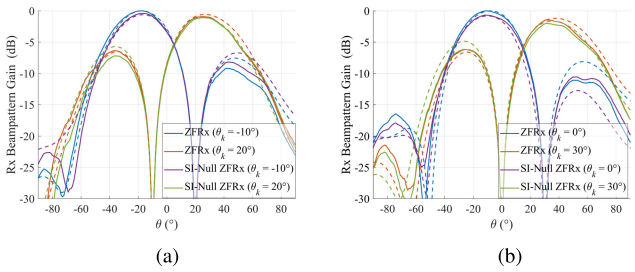


FIGURE 11. Simulation (dashed) and measurement (solid) results for conventional and proposed ZFRx beamformers: normalized Rx gain beam patterns steered to (a) $\theta_k = -10^\circ$ and $\theta_k = 20^\circ$, and (b) $\theta_k = 0^\circ$ and $\theta_k = 30^\circ$.

downlink beams are simultaneously formed. Consequently, the Rx beamformer operates in the presence of the residual SI produced by the constrained Tx solution. Under these conditions, the proposed SI-Null ZFRx maintains accurate main-lobe alignment with less than 1 dB peak degradation and only moderate sidelobe variation compared to conventional ZFRx. In addition to beam shaping, the null-space projection significantly improves the overall system isolation. While near-complete SI suppression is achieved in simulation, measurements show approximately 80 dB isolation in practice due to SI channel measurement errors, DAC/ADC nonlinearities, and modeling imperfections. Despite these limitations, the achieved suppression provides a substantial isolation margin and demonstrates the feasibility of IBFD MU-MIMO operation under strong coupling conditions with sufficient spatial DoF.

C. PRACTICAL CONSIDERATIONS

From a practical deployment perspective, the Tx–to–Rx coupling matrix does not require continuous re-estimation. Since the coupling environment typically varies much more slowly than the wireless communication channel, the calibrated or estimated coupling matrix can often be reused over extended periods. Only environmental changes that significantly modify the coupling characteristics require recalibration or updated SI channel estimation, whereas the communication beamformers can continue to be updated at the normal channel coherence rate.

The proposed framework also exhibits favorable computational scalability. The eigenvalue decomposition required to identify the low-coupling Tx subspace is performed only when the coupling matrix is updated, with complexity on the order of $O(N^3)$. Subsequently, the Tx and Rx beamforming weights are obtained using the closed-form formulations in Section III, with the online complexity dominated by conventional ZF operations that scale with the reduced Tx subspace dimension L and the number of served users K. Consequently, the online computational burden remains comparable to that of conventional ZF beamforming while explicitly enforcing the desired SI isolation constraint.

VI. CONCLUSION

This work presented a measurement-driven beamforming framework for IBFD MU-MIMO antenna arrays that integrates explicit SI control with simultaneous multi-user communication. By constructing the Tx beamformer within a measured low-coupling spatial subspace and applying receive-side null-space projection, the proposed framework enables simultaneous multi-user beamforming while maintaining controllable SI levels. Full-wave simulations and RFSoC-based measurements demonstrated substantial Tx-to-Rx and system-level SI suppression under strong coupling conditions with only moderate degradation in beamforming performance. The proposed formulation provides closed-form Tx and Rx beamformers derived directly from measured coupling and communication channel matrices, avoiding iterative optimization while explicitly revealing the trade-off between SI isolation, available spatial DoF, and beamforming performance. These results demonstrate a practical and scalable beamforming strategy for future IBFD MU-MIMO systems.

REFERENCES

[1] D. Erricolo, D. S. Filipovic, K. Haneda, and Z. Zhang, "Guest editorial special issue on antennas and propagation aspects of in-band full-duplex applications," *IEEE Trans. Antennas Propag.*, vol. 69, no. 11, pp. 7085–7091, Nov. 2021.

[2] B. Smida, R. Wichman, K. E. Kolodziej, H. A. Suraweera, T. Riihonen, and A. Sabharwal, "In-band full-duplex: The physical layer," *Proc. IEEE*, vol. 112, no. 5, pp. 433–462, May 2024.

[3] G. C. Alexandropoulos, M. A. Islam, and B. Smida, "Full-duplex massive multiple-input, multiple-output architectures: Recent advances, applications, and future directions," *IEEE Veh. Technol. Mag.*, vol. 17, no. 4, pp. 83–91, Dec. 2022.

[4] T. Le-Ngoc, Y. Gong, and M. Mahmood, *Half-Duplex/Full-Duplex MU-mMIMO: Metamaterial-Based Large-Scale Array & Hybrid Beamforming Design*. Cham, Switzerland: Springer, 2026.

[5] J. Kim, W. Choi, and H. Park, "Beamforming for full-duplex multiuser MIMO systems," *IEEE Trans. Veh. Technol.*, vol. 66, no. 3, pp. 2423–2432, Mar. 2017.

[6] M. Abdelghaffar, T. V. P. Santhappan, Y. Tokgoz, K. Mukkavilli, and A. Tingfang Ji, "Subband full-duplex large-scale deployed network designs and tradeoffs," *Proc. IEEE*, vol. 112, no. 5, pp. 487–510, May 2024.

[7] K. E. Kolodziej, B. T. Perry, and J. S. Herd, "In-band full-duplex technology: Techniques and systems survey," *IEEE Trans. Microw. Theory Techn.*, vol. 67, no. 7, pp. 3025–3041, Jul. 2019.

[8] E. Everett, A. Sahai, and A. Sabharwal, "Passive self-interference suppression for full-duplex infrastructure nodes," *IEEE Trans. Wireless Commun.*, vol. 13, no. 2, pp. 680–694, Feb. 2014.

[9] M. V. Kuznetcov, S. K. Podilchak, A. J. McDermott, and M. Sellathurai, "Dual-polarized high-isolation antenna design and beam steering array enabling full-duplex communications for operation over a wide frequency range," *IEEE Open J. Antennas Propag.*, vol. 2, pp. 521–532, 2021.

[10] S. Khaledian, F. Farzami, B. Smida, and D. Erricolo, "Inherent self-interference cancellation for in-band full-duplex single-antenna systems," *IEEE Trans. Microw. Theory Techn.*, vol. 66, no. 6, pp. 2842–2850, Jun. 2018.

[11] T. Wu, F. Zeng, X. Yang, W. Guo, and Z. Zhang, "Highly-integrated dual-polarized multibeam mm-wave array antenna with ultra-high Tx–Rx isolation for in-band full duplex (IBFD) application," *IEEE Open J. Antennas Propag.*, vol. 6, pp. 1348–1357, 2025.

[12] S. B. Venkatakrishnan, A. Hovsepian, and J. L. Volakis, "Antenna agnostic feed cancellation STAR system for improved cancellation," *URSI Radio Sci. Bull.*, vol. 2020, no. 374, pp. 46–53, Sep. 2020.

[13] E. Everett, C. Shepard, L. Zhong, and A. Sabharwal, "SoftNull: Many-antenna full-duplex wireless via digital beamforming," *IEEE Trans. Wireless Commun.*, vol. 15, no. 12, pp. 8077–8092, Dec. 2016.

[14] R. Ziegahn and T. Le-Ngoc, "Joint transmit and receive beamforming design for joint multi-user interference and self-interference rejection for full-duplex sub-connected MU-mMIMO," in *Proc. IEEE Wireless Commun. Netw. Conf. (WCNC)*, Mar. 2025, pp. 1–6.

[15] X. Chen, V. Savaux, M. Crussière, P. Savelli, and K.-C. Yao, "Self-interference cancellation for MIMO full-duplex downlink systems: A constrained MMSE-based precoding approach," *IEEE Access*, vol. 13, pp. 57030–57042, 2025.
[16] Y. Gong and T. Le-Ngoc, "Nulling steering beamforming for Tx–Rx isolation optimization in full-duplex mMIMO," in *Proc. GLOBECOM IEEE Global Commun. Conf.*, Dec. 2024, pp. 891–896.
[17] M. A. Islam, G. C. Alexandropoulos, and B. Smida, "Simultaneous downlink data transmission and uplink channel estimation with re- duced complexity full duplex MIMO radio," in *Proc. IEEE Int. Conf. Commun. Workshops (ICC Workshops)*, 2020, pp. 1–6.
[18] J. Mirza, G. Zheng, K.-K. Wong, S. Lambotharan, and L. Hanzo, "On the performance of multiuser MIMO systems relying on full-duplex CSI acquisition," *IEEE Trans. Commun.*, vol. 66, no. 10, pp. 4563–4577, Oct. 2018.
[19] M. Ayebe, R. Maaskant, S. E. Gunnarson, J. Malmström, M. Ivashina, and H. Holter, "Joint Tx–Rx beamforming for optimal gain and self-interference mitigation in in-band full-duplex arrays: Theory, figures of merit, and validation," *IEEE Antennas Wireless Propag. Lett.*, vol. 24, pp. 1317–1321, 2025.
[20] K. Kurokawa, "Power waves and the scattering matrix," *IEEE Trans. Microw. Theory Techn.*, vol. MTT-13, no. 2, pp. 194–202, Mar. 1965.
[21] K. F. Warnick, D. B. Davidson, and D. Buck, "Embedded element pattern loading condition transformations for phased array modeling," *IEEE Trans. Antennas Propag.*, vol. 69, no. 3, pp. 1769–1774, Mar. 2021.
[22] A. Ludwig, "The definition of cross polarization," *IEEE Trans. Antennas Propag.*, vol. AP-21, no. 1, pp. 116–119, Jan. 1973.
[23] C. B. Peel, B. M. Hochwald, and A. L. Swindlehurst, "A vector-perturbation technique for near-capacity multiantenna multiuser communication—Part I: Channel inversion and regularization," *IEEE Trans. Commun.*, vol. 53, no. 1, pp. 195–202, Jan. 2005.
[24] S.-R. Lee, J.-S. Kim, S.-H. Moon, H.-B. Kong, and I. Lee, "Zero-forcing beamforming in multiuser MISO downlink systems under per-antenna power constraint and equal-rate metric," *IEEE Trans. Wireless Commun.*, vol. 12, no. 1, pp. 228–236, Jan. 2013.
[25] M. Joham, K. Kusume, M. H. Gzara, W. Utschick, and J. A. Nossek, "Transmit Wiener filter for the downlink of TDDDS-CDMA systems," in *Proc. IEEE 7th Int. Symp. Spread Spectr. Techn. Appl.*, vol. 1, Sep. 2002, pp. 9–13.
[26] M. Joham, W. Utschick, and J. A. Nossek, "Linear transmit processing in MIMO communications systems," *IEEE Trans. Signal Process.*, vol. 53, no. 8, pp. 2700–2712, Aug. 2005.
[27] M. Ayebe, R. Maaskant, J. Malmström, S. E. Gunnarson, H. Holter, and M. Ivashina, "3D-printed silver-coated Vivaldi array with integrated coaxial probe feeding," in *Proc. IEEE Int. Symp. Antennas Propag. INC/USNC-URSI Radio Sci. Meeting (AP-S/INC-USNC-URSI)*, Jul. 2024, pp. 7–8.
[28] M. Ayebe et al., "In-band full-duplex antenna beamforming and synchronization for self-interference mitigation: Multi-tile RFSoC testbed design and deployment," in *Proc. 19th Eur. Conf. Antennas Propag. (EuCAP)*, Mar. 2025, pp. 1–5.



MUSTAFA AYEBE (Student Member, IEEE) received the B.S. and M.S. degrees in electrical and electronics engineering from Ozyegin University, Istanbul, Türkiye, in 2020 and 2022, respectively. He is currently pursuing the Ph.D. degree in electrical engineering with the Chalmers University of Technology, Gothenburg, Sweden, with a focus on in-band full-duplex antenna arrays, self-interference suppression, and antenna design for wireless communication and radar applications. He received the IEEE AP-S Acharya Jagadish Chandra Bose Paper Award in 2026 for his contributions to full-duplex antenna array research.



ROB MAASKANT (Senior Member, IEEE) received the M.Sc. and Ph.D. degrees (cum laude) in electrical engineering from Eindhoven University of Technology (TU/e), Eindhoven, The Netherlands, in 2003 and 2010, respectively.

From 2002 to 2010, he was with Netherlands Institute for Radio Astronomy (ASTRON), Dwingeloo, The Netherlands, where he worked as an Antenna Researcher. Since 2010, he has been with the Antenna Group, Department of Electrical Engineering, Chalmers University of Technology, Gothenburg, Sweden, where he is currently a Professor. He has held prestigious research fellowships and grants, including a Marie Skłodowska-Curie Fellowship (Rubicon, NWO), and faculty positions at both TU/e and Chalmers supported by competitive funding programs. He is the Primary Developer of the CAESAR software, an advanced integral-equation-based solver for the analysis of large-scale antenna array systems. His research focuses on the analysis and design of integrated antenna systems, including reconfigurable intelligent surfaces (RIS) and full-duplex integrated sensing and communication (ISAC) for next-generation wireless systems.

Dr. Maaskant has served on the Antennas and Propagation Community as an Associate Editor for IEEE TRANSACTIONS ON ANTENNAS AND PROPAGATION, IEEE ANTENNAS AND WIRELESS PROPAGATION LETTERS, and *Forum for Electromagnetic Research Methods and Application Technologies*.



BO GÖRANSSON (Member, IEEE) received the M.Sc. degree in applied physics and electrical engineering from Linköping University, Sweden, in 1991, and the Ph.D. degree in array signal processing from the KTH Royal Institute of Technology, Stockholm, Sweden, in 1997.

He joined Ericsson Research in 1998, where he was working with research and standardization of 3G, 4G, and 5G physical layer with special interest in MIMO and beamforming technologies. Since 2008, he has been with AI & Technology Foresight, a research group within business unit networks, where he worked on 4G and 5G testbeds. During this time, he was also involved in standardizing OTA radio requirements for antenna-integrated radio systems. Since 2019, he has been an Adjunct Professor with the KTH Royal Institute of Technology. He is currently a Senior Expert in multi-antenna systems and architectures with Ericsson. He holds more than 200 patents (issued and pending). His research interest is to understand massive MIMO systems from the physical layer all the way to radiated RF. He received the Ericsson Inventor of the Year Award in 2012.



HENRIK HOLTER (Member, IEEE) has been with Ericsson since 2021, where he is a Principal Developer, researching hardware and signal processing for integrated sensing and communication (ISAC) and wireless communication. He was with SAAB 2001–2021, where he researched electronic warfare and radar systems, the last five years as the Head of research and technology at the SAAB Electronic Warfare Unit.